Numerical study of the stability regions for half-quantum vortices in superconducting Sr_2RuO_4

KEVIN ROBERTS

University of Illinois,

Department of Physics

1110 W. Green St.

Urbana, IL 61801 USA

E-mail: krobert7@illinois.edu

RAFFI BUDAKIAN

University of Illinois,

Department of Physics

1110 W. Green St.

Urbana, IL 61801 USA

E-mail: budakian@illinois.edu

MICHAEL STONE

University of Illinois,

Department of Physics

1110 W. Green St.

Urbana, IL 61801 USA

E-mail: m-stone5@illinois.edu

Abstract

We numerically solve the coupled Landau-Ginzburg-Maxwell equations for a model of a spin triplet $p_x + ip_y$ superconductor in which whole or half-quanta of flux thread through a hole. We recover the pattern of stable and unstable regions for the half-flux quanta observed in a recent experiment.

PACS numbers: 74.20.De,74.20.Rp,74.25.Ha,74.70.Pq

I. INTRODUCTION

Superconductors with triplet $p_x + ip_y$ pairing are interesting because they can host half-quantum vortices with Majorana core states and non-Abelian braid statistics [1–3]. There is indirect evidence that the layered superconductor Sr_2RuO_4 has this pairing [4], and a search is on for "smoking gun" signatures that will confirm this. One signature — chiral edge currents — has proved elusive, but recent work [5] has found striking results suggesting that half-quantum vortices have been detected. If this result is correct, it strongly supports the spin triplet pairing character of the superconducting order parameter.

In the experiment reported in [5] a micron-sized annular flake of Sr_2RuO_4 is mounted on a cantilever. Its magnetic moment is monitored as magnetic fields both perpendicular (B_x) and parallel (B_z) to the c-axis are applied. As B_z is increased, moment jumps corresponding to the entry of single-flux-quantum vortices into the hole in the annulus are easily observed (see figure 1).
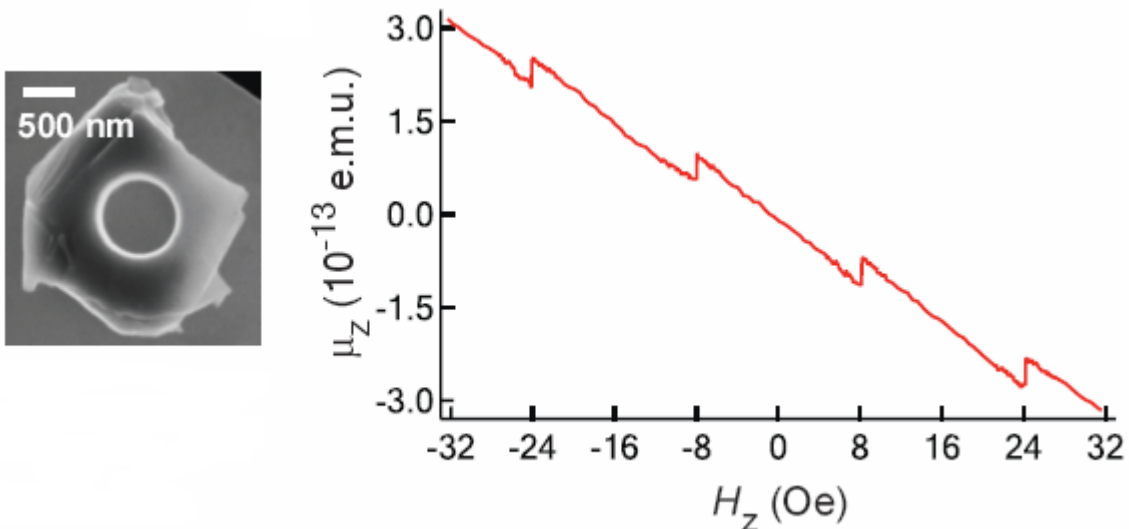

FIG. 1: SRO sample and magnetization curves showing integer flux transitions adapted from [5].

When a sufficiently large in-plane field B_x is applied, these entry-event jumps break up into two separate events, each with one-half of the original magnetic-moment jump. (See Figure 2.)

The most obvious explanation is that we are seeing half-quantum vortices: The large B field presumably has broken a spin orbit coupling that had held the spin-triplet order-parameter **d** vector parallel to the pair angular momentum vector **l**. The **d** vector can now
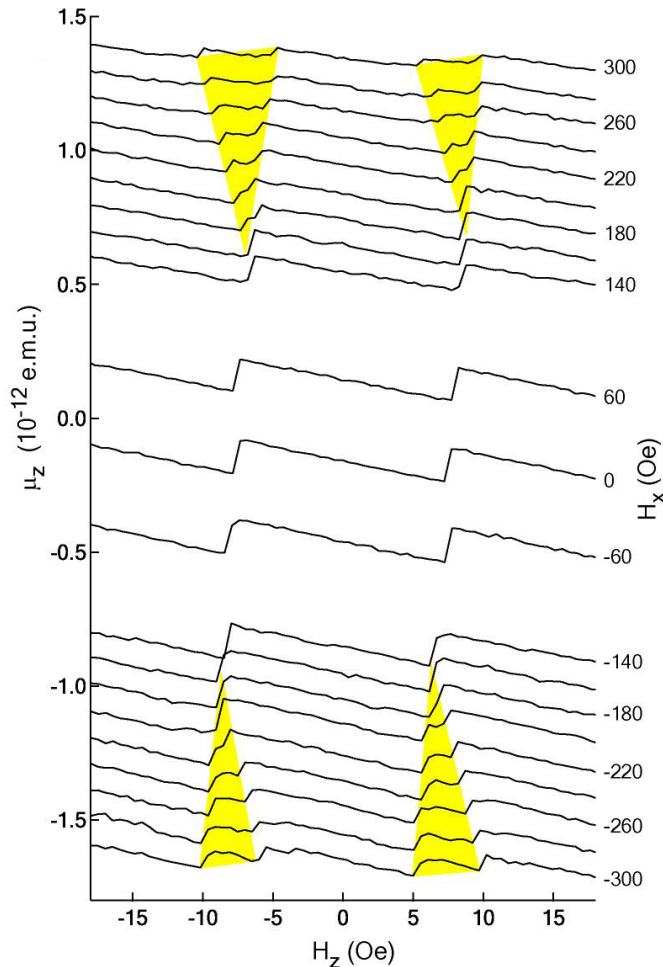
FIG. 2: Magnetization curves for various values of applied in-plane field. Adapted from [5]. The shaded region highlights the wedge shaped character of the half-flux state's stability region.

rotate freely in the x-z plane and this freedom permits the existence of a half-quantum vortex defect around which the $\mathbf{d}$ vector and the order-parameter phase ϕ both rotate through an angle π while leaving the spin-triplet order parameter single valued. These rotations have the effect of producing a phase-winding vortex in one spin component, while leaving the other with no phase winding. A circulating "anti-vortex" current is nonetheless induced in the second spin component by the magnetic field, and at large distance the spin-up and spin-down flow velocities become equal and opposite. This means that there is a long-range spin current surrounding the vortex. It is the necessity of reducing the logarithmically divergent free-energy-cost of this spin current that mandates the use of small annular samples [6].

As B_x is increased, the separation between the half-quantum jumps becomes larger. Vakaryuk and Leggett [7] have proposed that this phenomenon can be explained by a *kine-*

matic spin polarization. The different flow velocities for the up and down spin condensates give rise to an analogue of the Bernoulli effect which increases the magnitude of the order parameter for one condensate and decreases it for the other. The resulting magnetic polarization lies parallel to B_x, and so alters the energy cost for a vortex to enter the sample. Assessing whether or not the energy gain from Vakaryuk-Leggett mechanism is sufficient to explain the experimental data requires a detailed accounting of the energy in the three dimensional magnetic field surrounding the sample and in the degree of polarization of the condensate. In this paper we perform this accounting by obtaining numerical solutions to an appropriate set of coupled Maxwell-Landau-Ginzburg-equations. With the specific geometry of the samples used in the experiment, and with reasonable values of the Landau-Ginzburg parameters, we find that we are able to qualitively reproduce the experimental data.

In section II we assemble the ingredients of the two-component Landau-Ginzburg free-energy functional that we use to model the superconductivity. In section III we explain how we find the field configurations that minimize our free energy functional, and how we extract from them magnetization curves that we can compare with the experimental data. Section IV presents the numerical results, and, finally, section V contains a brief discussion of these results and their significance.

II. TWO-COMPONENT LANDAU-GINZBURG FORMALISM

A. Spin and charge stiffness

For a spin-triplet $p_x + ip_y$ superconductor with a fixed orbital angular momentum vector $\mathbf{l} = \hat{\mathbf{z}}$, the order parameter is matrix-valued and of the form

$$\begin{bmatrix} \Delta_{\uparrow\uparrow} & \Delta_{\uparrow\downarrow} \\ \Delta_{\downarrow\uparrow} & \Delta_{\downarrow\downarrow} \end{bmatrix} = |\Delta|e^{i\chi}(-i\sigma_2\,\boldsymbol{\sigma}\cdot\mathbf{d}) = |\Delta|e^{i\chi}\begin{bmatrix} -(d_1+id_2) & d_3 \\ d_3 & d_1-id_2 \end{bmatrix}. \qquad (1)$$

The $\mathbf{d}$ vector has unit length, and for our application we will assume that it is perpendicular to a spin-quantization axis $\mathbf{e_3}$, which need not be the z axis. We therefore set $d_3 = 0$, $d_1 + id_2 = e^{i\phi}$, and define the phases of $\Delta_{\uparrow\uparrow}$ and $\Delta_{\downarrow\downarrow}$ to be $\theta_\uparrow + \pi$ and $\theta_\downarrow$ respectively. Then

$$\chi = \frac{1}{2}(\theta_\uparrow + \theta_\downarrow), \qquad (2)$$

$$\phi = \frac{1}{2}(\theta_\uparrow - \theta_\downarrow). \qquad (3)$$

The authors of [6] write the free-energy density in the London form

$$K_{\text{london}} = \rho_s \left| \nabla\chi - \frac{2e}{\hbar}\mathbf{A} \right|^2 + \rho_{\text{spin}}|\nabla\phi|^2. \tag{4}$$

This expression contains only the Goldstone fields χ and ϕ and so ignores the free-energy cost of gradients in the magnitude of the order parameter. Nonetheless (4) captures the essential far-from-core vortex energetics. In particular, in a half-quantum vortex either $\theta_\uparrow$ or $\theta_\downarrow$ (but not both) rotate through $\pm 2\pi$. Then χ and ϕ rotate through $\pm\pi$. Far from the vortex core the $\mathbf{B}$ field will adjust so as to make the first term in K zero, so the total flux threading the half-vortex is given by

$$\Phi_{1/2} = \oint \mathbf{A}\cdot d\mathbf{r} = \frac{\hbar}{2e}\oint \nabla\chi\cdot d\mathbf{r} = \frac{1}{4}\left(\frac{2\pi\hbar}{e}\right) = \frac{1}{2}\Phi_0. \tag{5}$$

The remaining term *cannot* be screened by the $\mathbf{B}$ field and gives a contribution to the vortex energy that is logarithmically divergent at large distance. This divergent energy cost means that a half-quantum vortex be disfavoured unless the spin stiffness ρ_{spin} is small and a finite size to the superconducting region cuts-off the long-distance contribution.

The angle-valued Goldstone fields are not suitable for numerical work as they are not singled-valued in the presence of vortices. We need to write the free energy in terms single-valued fields. We therefore introduce fields $\psi_\uparrow = |\psi_\uparrow|\exp\{i\theta_\uparrow\}$ and $\psi_\downarrow = |\psi_\downarrow|\exp\{i\theta_\downarrow\}$. The simplest form for the Landau-Ginzburg free-energy density that has the correct symmetries contains the kinetic-energy density

$$K_{\text{landau}} = \frac{\hbar^2}{2m^*}\left\{\left|\left(\nabla - \frac{2ie}{\hbar}\mathbf{A}\right)\psi_\uparrow\right|^2 + \left|\left(\nabla - \frac{2ie}{\hbar}\mathbf{A}\right)\psi_\downarrow\right|^2 + 2b\mathbf{J}_\uparrow\cdot\mathbf{J}_\downarrow\right\}, \tag{6}$$

where

$$\mathbf{J}_\uparrow = \frac{ie\hbar}{m^*}\left(\psi_\uparrow^*\left(\nabla - \frac{2ie}{\hbar}\mathbf{A}\right)\psi_\uparrow - \psi_\uparrow\left(\nabla + \frac{2ie}{\hbar}\mathbf{A}\right)\psi_\uparrow^*\right), \tag{7}$$

$$\mathbf{J}_\downarrow = \frac{ie\hbar}{m^*}\left(\psi_\downarrow^*\left(\nabla - \frac{2ie}{\hbar}\mathbf{A}\right))\psi_\downarrow - \psi_\downarrow\left(\nabla + \frac{2ie}{\hbar}\mathbf{A}\right)\psi_\downarrow^*\right). \tag{8}$$

The current-current interaction introduces no new magnitude-gradient free-energy cost, and so does not affect the coherence length.

If we set $\psi_\uparrow = |\psi|e^{i\theta_\uparrow}$, *etc.*, and temporarily ignore derivatives of the common magnitude $|\psi|$, then

$$K_{\text{landau}} \approx |\psi|^2\frac{\hbar^2}{2m^*}\left\{\left|\nabla\theta_\uparrow - \frac{2e}{\hbar}\mathbf{A}\right|^2 + \left|\nabla\theta_\downarrow - \frac{2e}{\hbar}\mathbf{A}\right|^2 + 2b\left(\nabla\theta_\uparrow - \frac{2e}{\hbar}\mathbf{A}\right)\cdot\left(\nabla\theta_\downarrow - \frac{2e}{\hbar}\mathbf{A}\right)\right\}$$

$$= \quad |\psi|^2 \frac{\hbar^2}{2m^*} \left\{ 2(1+b) \left| \nabla\chi - \frac{2e}{\hbar}\mathbf{A} \right|^2 + 2(1-b)|\nabla\phi|^2 \right\}, \tag{9}$$

which is to be compared with desired London form of [6]. As ρ_{spin} must be positive, b must be less than unity. Being just less than unity encourages half-quantum vortices.

The presence the term $2b\mathbf{J}_\uparrow \cdot \mathbf{J}_\downarrow$ in the free energy density alters the current $\mathbf{J}_{\mathrm{maxwell}}$ that couples to the magnetic field. We have

$$\mathbf{J}_{\mathrm{maxwell}} = \mathbf{J}_\uparrow + \mathbf{J}_\downarrow - \frac{8e^2 b}{m^*}(|\psi_\uparrow|^2 \mathbf{J}_\downarrow + |\psi_\downarrow|^2 \mathbf{J}_\uparrow). \tag{10}$$

B. Kinematic spin polarization

Legget and Vakaryuk propose [7] that the dependence of the half quantum vortex stability region on the applied in-plane field B_x can be understood via the existence of a spontaneous spin polarization in the half quantum vortex state that arises from the difference between the spin-up and spin-down condensate velocities $\mathbf{v}_\uparrow$ and $\mathbf{v}_\downarrow$ in the half-quantum vortex.

The polarization occurs because for each of the two spin components in the Landau-Ginzburg theory we have a version of Bernoulli's equation:

$$\frac{1}{2}m^*|\mathbf{v}_{\uparrow,\downarrow}|^2 + \frac{\partial u}{\partial \rho_{\uparrow,\downarrow}} = \mathrm{const.} \tag{11}$$

Here $\rho_{\uparrow,\downarrow} = |\psi_{\uparrow,\downarrow}|^2$, and

$$u(\rho) = \alpha\rho + \frac{1}{2}\beta\rho^2, \tag{12}$$

is the potential part of the Landau-Ginzburg free energy density.

As a consequence, the faster the superflow, the lower the order-parameter density. The polarizing tendency is proportional to

$$|\mathbf{v}_\uparrow|^2 - |\mathbf{v}_\downarrow|^2 = (\mathbf{v}_\uparrow + \mathbf{v}_\downarrow) \cdot (\mathbf{v}_\uparrow - \mathbf{v}_\downarrow) \tag{13}$$

$$= \mathbf{v}_{\mathrm{charge}} \cdot \mathbf{v}_{\mathrm{spin}} \tag{14}$$

This polarizing tendency gives rise to spin magnetic moment

$$\boldsymbol{\mu}_{\mathrm{spin}} = g\mu_B \left(|\psi_\uparrow|^2 - |\psi_\downarrow|^2 \right) \mathbf{e}_3 \tag{15}$$

Here μ_B denotes the Bohr magneton, and g is a phenomenological parameter that we expect to be of order unity. (If $|\psi|^2_{\uparrow,\downarrow}$ were the actual density of cooper pairs, and if each of the two

electrons in the pair contributes a Dirac moment of $\mu_{\text{electron}} \approx \mu_B$, we would have $g = 2$.)
The induced moment couples to the magnetic field to give a free-energy contribution

$$\Delta F = -\mathbf{B} \cdot \boldsymbol{\mu}_{\text{spin}}. \tag{16}$$

Jang *et al.* [5] assume that this moment lies in the x-y plane and so it is affected only by B_x. We therefore account for it by including a term

$$\Delta F = -g\mu_B \left(|\psi_\uparrow|^2 - |\psi_\downarrow|^2 \right) |B_\parallel| \tag{17}$$

in our free-energy functional.

C. Anisotropy

The superconductor Sr_2RuO_4 is quite anisotropic, and it is necessary to replace the usual Landau-Ginzburg scalar mass m^* with a mass tensor M^* so that the free energy becomes

$$F[\psi, \psi^*, \mathbf{A}] = \int_\Omega d^3x \left\{ \frac{\hbar^2}{2} \left(\nabla + \frac{2ie}{\hbar} \mathbf{A} \right) \psi^* \cdot (M^*)^{-1} \cdot \left(\nabla - \frac{2ie}{\hbar} \mathbf{A} \right) \psi + \right.$$
$$\left. + \alpha |\psi|^2 + \frac{\beta}{2} |\psi|^4 + \frac{1}{2\mu_0} |\nabla \times \mathbf{A} - \mathbf{B}_{\text{ext}}|^2 \right\}. \tag{18}$$

We choose a coordinate system such that the crystal ab planes lie in the xy-plane and are displaced from each other in the z-direction. Then, the effective mass tensor takes the form

$$M^* = \text{diag}(m_\parallel, m_\parallel, m_\perp) \tag{19}$$

where the ratio

$$\frac{m_\perp}{m_\parallel} = \left(\frac{\lambda_\perp}{\lambda_\parallel} \right)^2 \tag{20}$$

can be calculated from the measured penetration depths $\lambda_\perp$ and $\lambda_\parallel$ of Sr_2RuO_4 and is found to be approximately 400.

III. NUMERICAL METHOD

Our goal is to create equilibrium magnetization curves that can be directly compared with those in [5] (see figures 1 and 2). Because of the asymmetric and three dimensional character of the experimental samples, these curves have to be found numerically.

For the numerical calculation, it is convenient to express the Landau-Ginzburg free energy in dimensionless form as

$$F[\psi_\uparrow, \psi_\downarrow, \mathbf{A}] = \int_\Omega d^3x \left\{ \sum_{\uparrow,\downarrow} \left[\left(\frac{\nabla}{\kappa} + i\mathbf{A} \right) \psi_i^* \cdot (M_{red}^*)^{-1} \cdot \left(\frac{\nabla}{\kappa} - i\mathbf{A} \right) \psi_i - |\psi_i|^2 + \frac{1}{2}|\psi_i|^4 \right] \right.$$
$$\left. + 2\tilde{b}\mathbf{J}_\uparrow \cdot (M_{red}^*)^{-1} \cdot \mathbf{J}_\downarrow + \tilde{\mu}(|\psi_\uparrow|^2 - |\psi_\downarrow|^2)B_{||} + |\nabla \times \mathbf{A} - \mathbf{B}_{ext}|^2 \right\} (21)$$

Here $\mathbf{J}_i = \mathrm{Re}\{-i\psi_i^*(\kappa^{-1}\nabla - i\mathbf{A})\psi^*\}$ is the dimensionless current, and $\tilde{b}$ and $\tilde{\mu}$ are dimensionless parameters corresponding to the current-current coupling b in (6) and $g\mu_B$ in (17), respectively. The parameter $\kappa \approx 2.3$ is the ratio of the in-plane penetration depth to the in-plane coherence length. Also

$$M_{red}^* = \mathrm{diag}(1, 1, m_\perp^*/m_{||}^*). \tag{22}$$

To find the magnetic field and condensate configurations that minimize the free energy functional (21) we used the commercial finite-element method solver COMSOL.
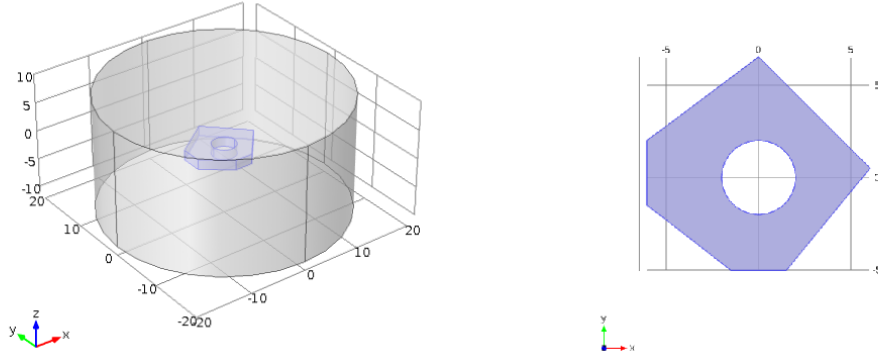

FIG. 3: On the left is shown a representation of the simulated geometry. On the right is a top-down view of the simulated ring. The axes in both figures are labelled in units of $\lambda_{||}$.

We will focus on the results for the single annular sample shown in figure 3. The ring's inner radius is 2 $\lambda_{||}$ while the outer radius averages 5.29 $\lambda_{||}$ where $\lambda_{||}(T = 0)$ is given as 152 nm for Sr_2RuO_4 in [4]. The height of the sample is 1.7 $\lambda_{||}$. This geometry is designed

9

to approximate the experimental sample shown in Figure [1]. The ring is centered in a cylindrical volume Ω of height 20 $\lambda_{\parallel}$ and radius 20 $\lambda_{\parallel}$. The dimensions of the cylinder were chosen to balance the competing effects of increased computation time for larger cylinders against spuriously high magnetic field energies caused by confining the field in too small a volume.

The externally imposed magnetic field $\mathbf{B} = (B_x, B_y, B_z)$ is established by imposing the inhomogeneous Dirichlet boundary condition

$$
\begin{aligned}
A_x &= \frac{1}{2}(B_y z - B_z y), \\
A_y &= \frac{1}{2}(B_z x - B_x z), \\
A_z &= \frac{1}{2}(B_x y - B_y x).
\end{aligned}
\tag{23}
$$

on the surface the $\partial\Omega$ of the cylinder.

The boundary conditions we impose on the order-parameter fields in (21) are the "natural" boundary conditions that arise from the variational problem of free energy minimization. In other words we require the vanishing of the integrated out variation terms on the surface of the superconductor. This leads to

$$
\begin{aligned}
\mathbf{n} \cdot (M_{\text{red}}^*)^{-1} \cdot \left(\frac{\nabla}{\kappa} - i\mathbf{A} - \frac{\tilde{\beta}}{\kappa} \mathbf{J}_\downarrow \right) \psi_\uparrow &= 0 \\
\mathbf{n} \cdot (M_{\text{red}}^*)^{-1} \cdot \left(\frac{\nabla}{\kappa} - i\mathbf{A} - \frac{\tilde{\beta}}{\kappa} \mathbf{J}_\uparrow \right) \psi_\downarrow &= 0
\end{aligned}
\tag{24}
$$

on the surface of the superconducting ring.

We find the fields that minimize the free energy by first choosing initial conditions for the magnetic vector potential and for the order-parameter fields, and then allowing them to relax to equilibrium. As the applied magnetic field along the z-axis is increased, we see vortices enter the superconductor and increase winding numbers about the ring. Each entry results in a discontinuous step in the magnetization. These transitions turn out to be difficult to model reliably. Although vortices enter the sample, the regions of metastabilty are large and geometry dependent. We therefore adopted a strategy that is similar to the field-cooling used in the actual experiments. We begin by imposing initial conditions

$$
\psi_\uparrow = \exp[in_\uparrow \phi]; \quad \psi_\downarrow = \exp[in_\downarrow \phi]
\tag{25}
$$

that correspond to a selected flux state. (Here, ϕ is the azimuthal angle around the ring. For instance, $(n_\uparrow, n_\downarrow) = (0,0)$ corresponds to the zero flux state while $(1,0)$ and $(0,1)$ correspond to half flux states.) After selecting the desired winding numbers, and setting the externally imposed magnetic field, we allow the system to relax to a local minimum of the free energy. This free energy is then calculated by evaluating the integral in (21). In this way we are able to construct diagrams of free energy versus applied magnetic field in the z-direction for different flux states and for different values of in-plane magnetic field. These diagrams reveal which flux state is energetically favourable at each value of applied z-axis field. Using these plots, we numerically compute the derivatives of the free energy with respect to the applied z-axis field, and thus construct the magnetization curves.
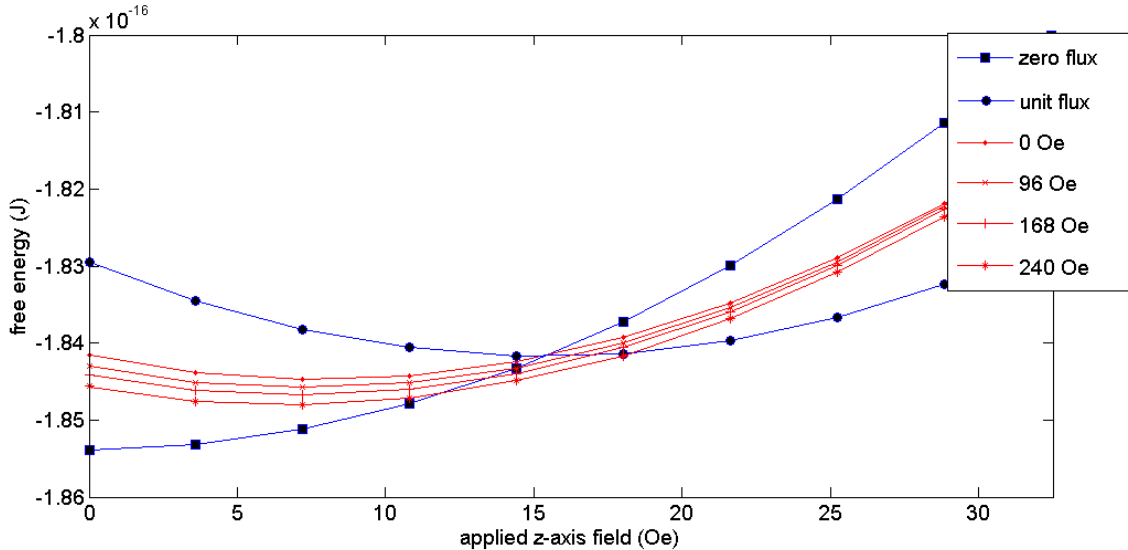
IV. RESULTS

FIG. 4: This figure shows an example of calculated relative free energies of the integer and half-flux states near the first transition. Each red line represents the free energy of the half-flux state at different values of applied in-plane magnetic field. Higher magnetic fields are seen to result in relatively lower free energies of the half-flux state.

Figure 4 illustrates the free energy of the system versus applied z-axis field (from 0 to 32.5 Gauss), and for a few values of applied in-plane magnetic field. The blue line depicts the (0,0) and (1,1) integer-flux states while the red line depicts the (1,0) half-flux state.[9]

11

One can see from the diagram that the half-flux state has a reduced free energy versus the integer-flux states for higher values of in-plane field.
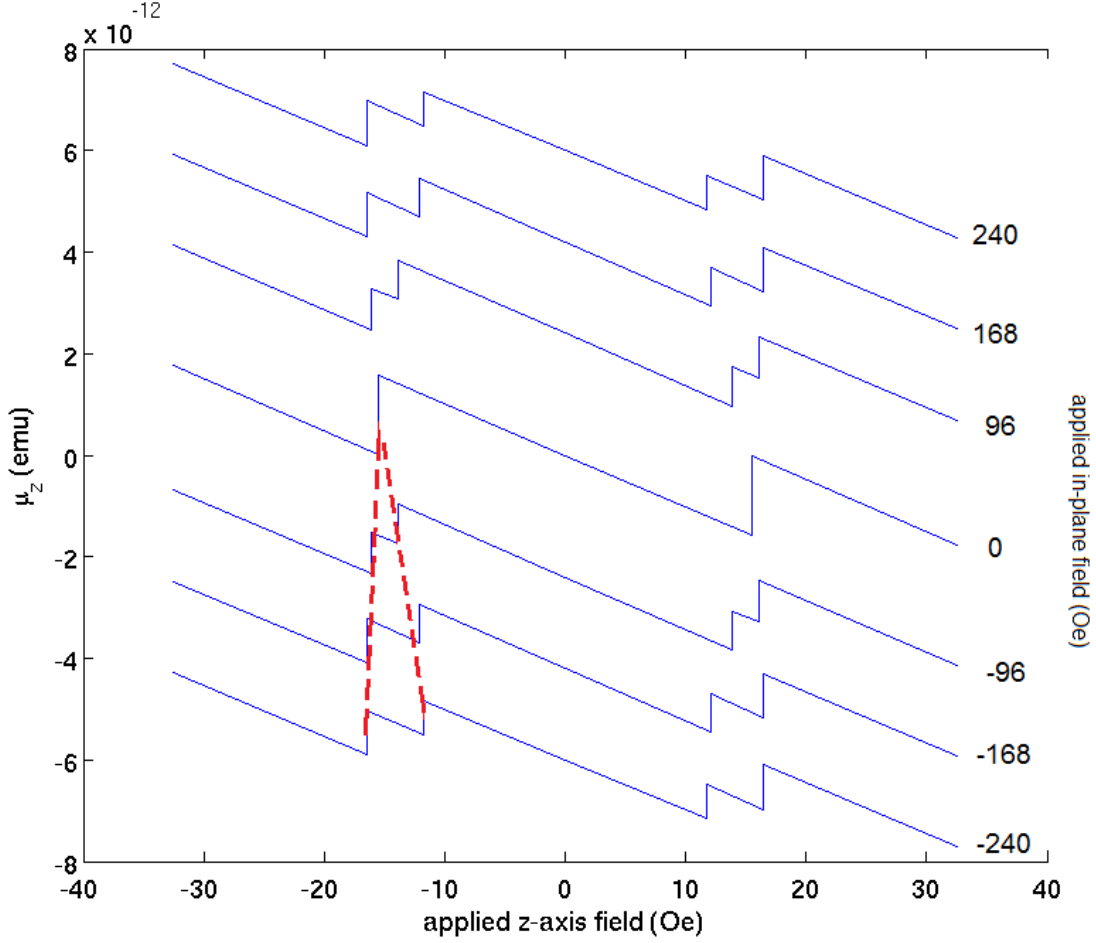

FIG. 5: Computed magnetization curves obtained using $\rho_{sp}/\rho_s = 0.25$ and a magnetic dipole moment of $0.55\mu_B$.

Applying a parabolic fit to the free energy curves, one can take the the derivative with respect to the applied magnetic field to obtain magnetization curves. Figure 5 displays magnetization curves versus z-axis field for various values of in-plane field as in Figure 2. The magnetization curves are seen to be qualitatively similar. By adjusting $\tilde{b}$ and $\tilde{\mu}$ one may obtain the desired minimum in-plane stabilization field and stability region growth rate.

The dimensionless current-current coupling parameter $\tilde{b}$ can be related to the ratio of the spin and charge fluid densities via

$$\frac{\rho_{sp}}{\rho_s} = \frac{1 - \tilde{b}}{1 + \tilde{b}}. \tag{26}$$

Typical values of $\tilde{b}$ which matched the experimental data were 0.4-0.6 corresponding to ρ_{sp}/ρ_s between 0.25 and 0.43.

If $\tilde{\mu}$ is interpreted as the magnetic dipole moment per particle of the spin condensate, it gives a magnetic dipole moment in units of $\sqrt{2}e^2 B_c \lambda^2 m_e^{-1}$. Using $B_c = 230$ Oe and $\lambda = 152$ nm, the value of this unit is approximately $2.12 \times 10^{-23} J/T \approx 2.2\mu_B$. Typical values of the magnetic dipole moment which fit the data were found to be around 0.6 μ_B.

The magnitude of the in-plane spin magnetic moment for the case of 240 Oe in-plane field is plotted in Figure 6. Near zero applied z-axis field the system is in the $(n_\uparrow, n_\downarrow) = (0,0)$ state. The presence of the in-plane magnetic field induces an in-plane magnetic moment even in the absence of kinematic spin polarization.Thus, there is a non-zero moment even in the integer flux states. The presence of kinematic spin polarization accounts for the sudden increase in moment at the transition to the half-flux state near 12 Oe. This additional moment vanishes when the system transitions to the unit fluxoid state at 16 Oe.

V. DISCUSSION

We have shown that the model described in section II can qualitatively reproduce the results of the experiment described in [5]. Using kinematic spin polarization and a current coupling term in a two-component Ginzburg-Landau model, numerical results show that an in-plane field results in the increasing stability of a half-quantum vortex state. This leads to a wedge-like stability region in the half-flux state versus applied c-axis field as shown in Figure 5. Moreover, this is achieved using physically reasonable values of μ and ρ_{sp}/ρ_s.

In comparing Figure 5 to Figure 2 there are some disrepencies that should be acknowledged. Firstly, the periodicity of the numerical result is approximately 30 Oe while that of the data is 16 Oe. This is due to the fact that, assuming a penetration depth of 152 nm, the simulated ring's hole diameter is 0.6 μm while the actual sample has a hole diameter of 0.75 μm. A smaller hole necessitates a larger applied field in order to achieve the flux necessary to induce a fluxoid transition.

A more perplexing difference is in the magnitude of the moments, the numerical result's moments being an order of magnitude larger than those shown in Figure 2. These small magentic moments seem to be found only in the smaller samples examined by Jang, et. al. The moment data collected from larger samples, as in Figure 2 of [8], seems to be of the
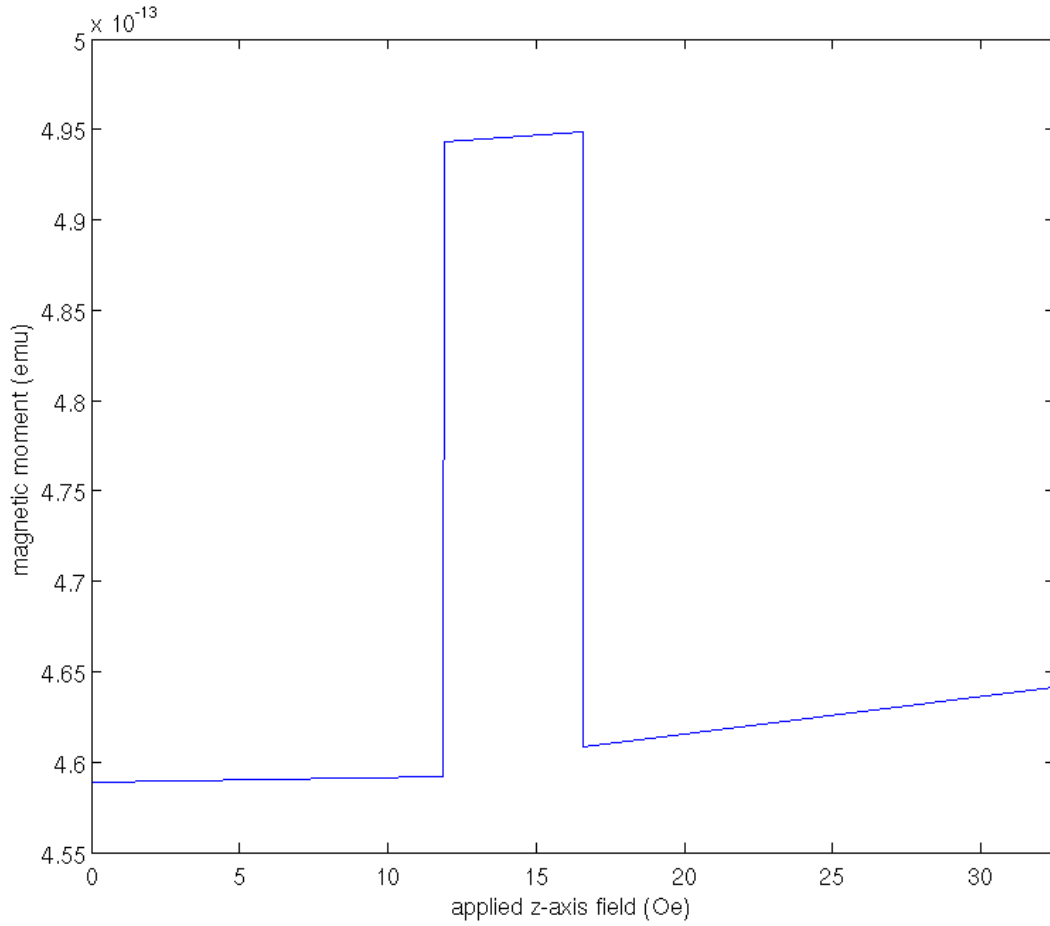
FIG. 6: The calculated in-plane spin magnetic moment for 200 Oe of applied in-plane field.

appropriate order of magnitude. At the present time, we can only speculate that the small moments are due to weakening of the superconductivity caused by crystal defects incurred during fabrication of the rings.

This discrepency in the magnitudes of the magnetic moments makes the interpretation of the experiments in [5] difficult. One possible scenario explaining the half-height jumps in magnetization were Abrikosov vortices piercing the side-wall nearly half-way between the top and bottom of the ring. One of the several arguments against this was that the magnitude of the induced spin magnetic moment μ_{HI} is an order of magnitude less than that produced by a side-wall vortex. The estimates of μ_{HI} were determined by Jang, et. al. by using the formula $\mu_{HI} = \delta H_z \Delta \mu_z / 4 (H_x - H_{x,min})$ where $\Delta \mu_z$ is the jump in magnetic moment upon entry of a unit vortex, δH_z is the width of the stability wedge, and $H_x - H_{x,min}$ is the amount

of applied in-plane field over the minimum necessary to see half-flux states. For the data shown in Figure 2, the implied $\mu_{HI} \approx 9 \times 10^{-15}$ emu while, from Figure 6, $\mu_{HI} \approx 3.5 \times 10^{-14}$ emu. So, since the measured $\Delta\mu_z$ and μ_{HI} appear to be poorly understood this argument loses some credibility. A better understanding will require an understanding of the character and stability of wall-vortex states.

VI. ACKNOWLEDGMENTS

---

[1] D. A. Ivanov, Phys. Rev. Lett, **86**, 268-7 (2001).

[2] A. Stern, F. von Oppen, E. Mariani, Phys. Rev. B **70**, 205338/1-13 (2004).

[3] M. Stone, S. B. Chung, Phys. Rev. **B73** 014505/1-11 (2006).

[4] For a review, see: A. P. Mackenzie, Y. Maeno, Rev. Mod. Phys. **75**, 657-712 (2003).

[5] J. Jang, D. G. Ferguson, V. Vakaryuk, R. Budakian, S. B. Chung, P. M. Goldbart, Y. Maeno, Science **333** 186-188 (2011).

[6] S. B. Chung, H. Bluhm, E.-A. Kim, Phys. Rev. Lett. **99**, 197002/1-4 (2007).

[7] V. Vakaryuk, A. J. Leggett Phys. Rev. Lett. **103**, 057003/1-4 (2009).

[8] J. Jang, R. Budakain, Y. Maeno, App. Phys. Lett. **98**, 132510 (2011)

[9] Applying an in-plane field produces a spin polarization for both both integer and half integer flux states. We have plotted the data so as to show the only the *relative* free energy of the integer and half integer states. We did this by shifting all curves by an in-plane-field dependent constant so that the integer-flux state's data overlap one another.